THE ASTROPHYSICAL JOURNAL, 421:87–91, 1994 January 20

HST OBSERVATIONS OF THE [O III] EMISSION-LINE REGION IN MARKARIAN 78[1]

A. CAPETTI,[2] F. MACCHETTO,[2,3] W. B. SPARKS,[2] AND A. BOKSENBERG[4]
Received 1993 April 19; accepted 1993 July 26

ABSTRACT

We present the results of *HST* observations of Mrk 78, a Seyfert 2 galaxy. Observations were taken with the Faint Object Camera using the F550M, F502M (which includes the [O III] $\lambda\lambda$4959, 5007 emission lines), and F130M filters. These are medium band filters centered at 5500, 5020, and 1300 Å, respectively. The [O III] image shows a biconical shape with a full opening angle of 40°, elongated in the direction of the radio structure, with its apex approximately coincident with the center of both the radio and optical continuum. A resolved (0.″8 in extent) obscuring region is present close to the center of the cone. The UV image confirms the result that emission from the nucleus is not seen directly. Our results provide a strong observational support for the "occultation/reflection" model for Seyfert 2 galaxies. We discuss the relation between radio and emission-line regions and propose a pure photoionization origin for the [O III] emission. Finally, we test the occultation model by comparing our observations with the *IRAS* data: a strongly anisotropic nuclear source is required to meet the energy requirement derived from the analysis of the far-infrared emission.

Subject headings: galaxies: individual (Markarian 78) — galaxies: nuclei — galaxies: Seyfert — ultraviolet: galaxies

1. INTRODUCTION

The study of polarized flux spectra has shown that at least some Seyfert 2 galaxies contain a hidden Seyfert 1 nucleus (Antonucci & Miller 1985; Miller & Goodrich 1990). It is thought that obscuring material, in the form of a thick obscuring torus, is oriented in a direction perpendicular to the radio emission: the structure of the torus allows photons generated in the central source to escape only along a cone aligned with the radio axis, providing also a common origin for the collimation of the relativistic plasma and the ultraviolet ionizing flux.

The anisotropy of the ionizing radiation is confirmed by the studies of Wilson, Baldwin, & Ulvestad (1985), Baldwin, Wilson, & Whittle (1987), Wilson, Ward, & Haniff (1988), and Kinney et al. (1991): the observed continuum cannot account for the number of recombination photons, suggesting that the ionizing continuum sources are not seen directly. The biconical structure of the emission-line region expected in this framework has been observed directly in a number of different sources, for example, by Tadhunter & Tsvetanov (1989), Pogge (1989), Evans et al. (1991), and Colina, Sparks, & Macchetto (1991). This overall picture is known as the "occultation/reflection" model for Seyfert 2 galaxies.

The mechanism responsible for ionizing the [O III] emitting gas is not fully understood, but the observed emission-line ratios are well explained by photoionization from a compact central source (Koski 1978) on gas clouds with densities ranging between 10^2 and 10^7 cm^{-3}. But contributions from shock heating or relativistic electrons can also play a role. In fact, Haniff, Wilson, & Ward (1988) found that, on a sample of 10 Seyfert galaxies which show an extended structure at radio wavelengths, the [O III] emission is always aligned within a few degrees to the radio axis, suggesting a connection between the relativistic and thermal gas. Pedlar et al. (1989) suggested that this association can be explained by radio-emitting components moving at 500 km s^{-1} compressing and heating interstellar gas through shock waves. It is therefore of great interest to investigate the relation between radio and optical emission-line regions in Seyfert 2 galaxies.

The high spatial resolution attainable with the *HST* Faint Object Camera offers a unique possibility to carry out detailed observations of the emission-line region and to investigate the gas morphology very close to the nucleus. As part of a program to investigate the nature of the emission-line region in Seyfert galaxies we have observed the Seyfert 2 galaxy Mrk 78, which has an extended narrow line emission region (NLR) with a double structure (Whittle et al. 1988).

Since the radio-emitting region is embedded within the NLR, it is essential to study their relationship to obtain a better understanding of both: our observations have produced images with a resolution similar to the VLA radio maps, making this comparison straightforward.

Details of the observations are given in § 2; the results are presented in § 3 and discussed in § 4. Summary and conclusions can be found in § 5. Throughout this paper we adopt $H_0 = 50$ km s^{-1} Mpc^{-1}. At a redshift $z = 0.0386$ Mrk 78 is at a distance of 231 h_{50}^{-1} Mpc, where 0.″1 corresponds to 110 h_{50}^{-1} pc.

2. OBSERVATIONS AND DATA REDUCTION

The observations were obtained with the Faint Object Camera (FOC) on 1992 September 19, in the f/96, 512 × 512 mode (Paresce 1992); the pixel size is 0.″022 corresponding to a field of view of 11″ × 11″. We used F130M, F502M, and F550M medium band filters with nominal exposure times of 3600 s for F130M and 1800 s for F502M and F550M. The F502M filter includes the redshifted [O III] $\lambda\lambda$4959, 5007 emission.

[1] Based on observations with the NASA/ESA *Hubble Space Telescope*, obtained at the Space Telescope Science Institute, which is operated by AURA, Inc., under NASA contract NAS 5-26555.

[2] Space Telescope Science Institute; 3700 San Martin Drive, Baltimore, MD 21218.

[3] Astrophysics Division, Space Science Department of ESA, Estec, NL-2200 AG Noordwijk, The Netherlands.

[4] Royal Greenwich Observatory, Madingley Road, Cambridge CB3 0EZ, UK.

The images were processed to correct for geometric distortion using the grid of regularly spaced reseaux marks on the detector photocathode; the data frames were then divided by normalized and geometrically corrected internal flat-field frames.

The redshifted wavelength of [O III] λ5007 for Mrk 78 is 5200 Å; the detector quantum efficiency of the F550M filter at this wavelength is 2.0×10^{-5}, compared with 1.2×10^{-2} for the F502M filter. Thus the F550M image does not contain any significant contribution from the emission line and can be used as a true measure of the continuum.

In order to subtract the continuum contribution from the F502M image we used the spectral information obtained by Kinney et al. (1991), obtained with a large aperture (15″) spectrograph. A power-law continuum ($F_\lambda = k\lambda^\beta$) was fitted to the spectrum, with a resulting $\beta = 1.97 \pm 0.20$. We then scaled the F550M continuum image to the F502M image using the known filter transmission curves taking into account the shape of the observed spectrum as just described. The scale factor obtained in this way is 0.82 ± 0.02. From both images we also subtract a constant background level determined by integrating in a region far from the source, and we then subtracted the scaled F550M image from the F502M image to obtain the image of the [O III] line emission alone.

We deconvolved the F502M and F550M images using Lucy's (1974) iterative algorithm and point-spread functions derived from the observations of the standard star BPM 16274. Convergence was achieved in 40 iterations.

3. RESULTS

Deconvolved images in the F502M and F550M filters are shown in Figures 1*a* and 1*b* (Plates 2 and 3), respectively. In the F502M image, which includes the [O III] line, the emission extends over 3″.5 × 6″.0 at the 3 σ level. This is comparable to the size observed in [O III] by Haniff et al. (1988) from the ground and allows us to use their image as a reference to determine the absolute position of our data.

Two regions of high luminosity within a fainter extended halo are seen in our data; they are located east and west of the galaxy's center and show smaller scale structures. The halo is more extended toward the west. In this region it has several bright knots and two bright arcs.

The total flux density in the F502M filter was computed using the internal calibration of the FOC: we obtained a flux of $4.09 \times 10^{-15} h_{50}^{-2}$ ergs cm^{-2} s^{-1} Å^{-1}.

The F550M image structure is similar to the F502M image, but the halo is less clearly visible due to the lower signal-to-noise in this image. The integrated flux is $2.98 \times 10^{-15} h_{50}^{-2}$ ergs cm^{-2} s^{-1} Å^{-1}.

Using the same correction for the shape of the continuum used to obtain the [O III] image, we derive a total [O III] emission of $2.63 \times 10^{-13} h_{50}^{-2}$ ergs cm^{-2} s^{-1}.

As discussed in § 2, we have also derived an [O III] image, shown in Figure 2. The main features in this image are the two bright regions already seen in the F502M image, showing a clear biconical shape.

In Figure 3 we show cross cuts 325 pixels wide (7″.1) taken along the cone axis of the F502M, F550M, and [O III] images; the western component is seen to be compact, but also fully resolved.

The cone has a full opening angle of $40° \pm 5°$, and its axis is at a position angle of $67° \pm 2°$ from the north. The central region of the cone is completely obscured in an area of 0″.8 in size along the E-W direction and displaced from the center of the cone by 0″.2.

Due to the low surface brightness and complex geometry of the extended halo we cannot determine accurately its position angle, but it appears to be well aligned with the cone.

The F130M filter, which includes Lyα, showed no emission from either the nucleus or the diffuse halo. The upper limit for the nucleus flux density can be estimated as 3.23×10^{-17} ergs cm^{-2} s^{-1} Å^{-1}, corresponding to a 6.6×10^{25} ergs s^{-1} Hz^{-1}.

4. DISCUSSION

4.1. *The* [O III] *Emission-Line Region*

For Mrk 78 Whittle et al. (1988) measured in the [O III] λ5007 line a total flux of $6.31 \times 10^{-13} h_{50}^{-2}$ ergs cm^{-2} s^{-1} and a flux of $1.91 \times 10^{-13} h_{50}^{-2}$ ergs cm^{-2} s^{-1} for the east and west compact components combined. We obtained a total flux in the [O III] $\lambda\lambda$4959, 5007 emission lines of $2.63 \times 10^{-13} h_{50}^{-2}$

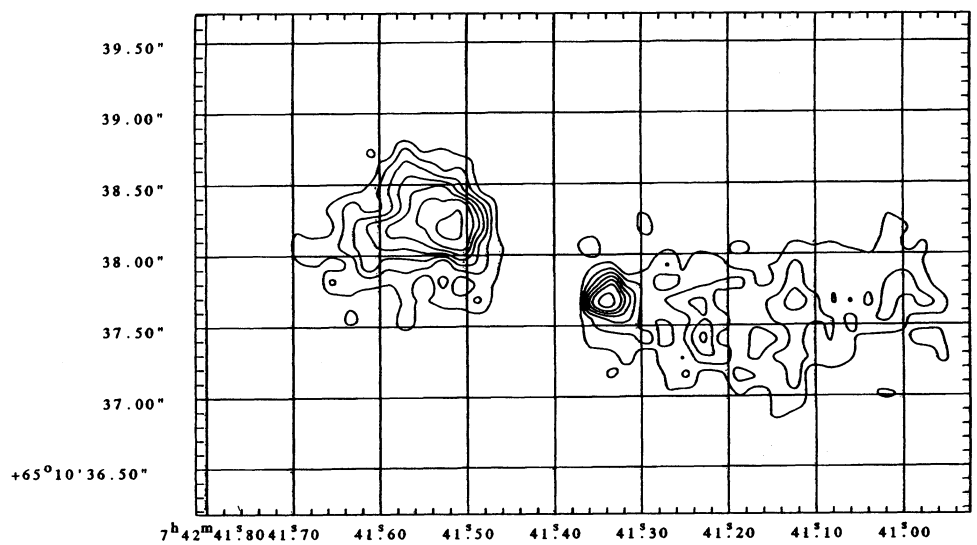

FIG. 2.—Contour plot of the [O III] emission-line region of Mrk 78. Contours levels are at 20%, 25%, 30%, 35%, 40%, 50%, 60%, 80% of the peak.

PLATE 2

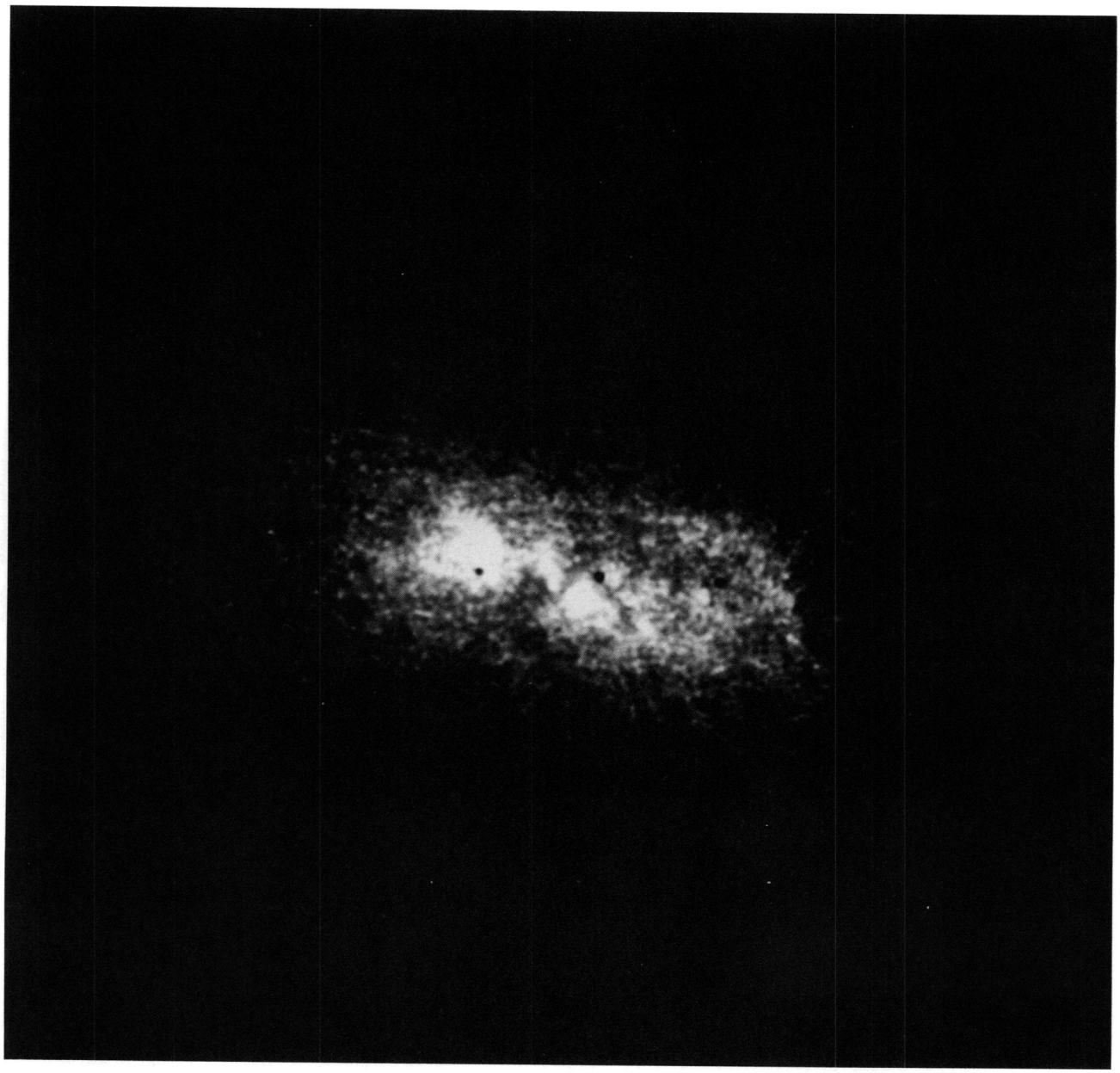

FIG. 1*a*

FIG. 1.—Deconvolved images of Mrk 78 in the F502M (*a*) and F550M (*b*) filters. North is at top and east to the left. The field of view is 5".5 × 5".5.

CAPETTI et al. (see 421, 88)

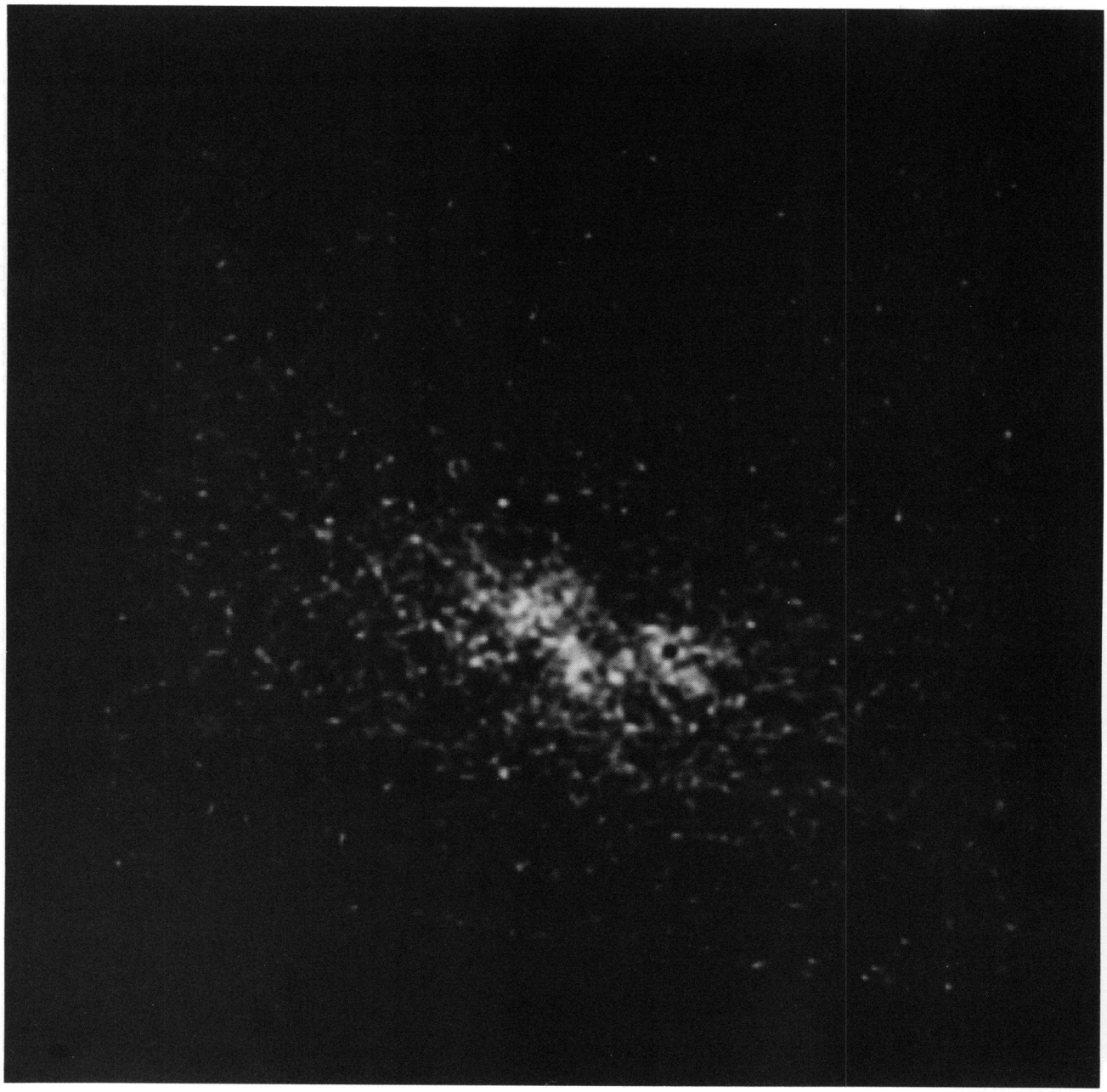

FIG. 1*b*

CAPETTI et al. (see 421, 88)

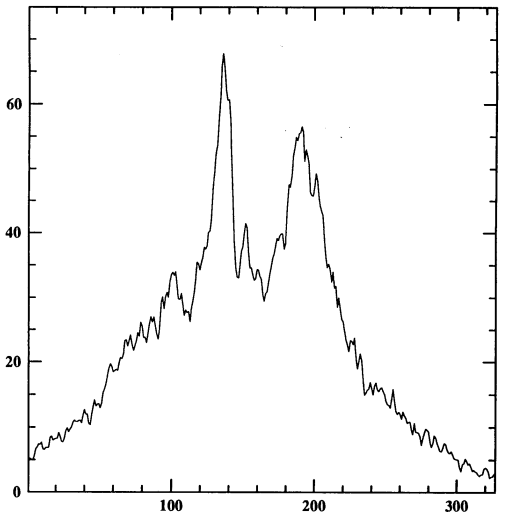

FIG. 3*a*

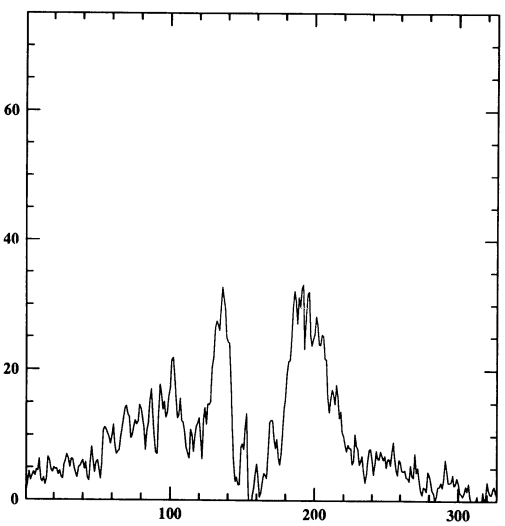

FIG. 3*c*

FIG. 3.—Cross cuts along the cone axis (P.A. +67°) of the F502M (*a*), F550M (*b*), and [O III] (*c*) images. The scale is in pixels (0.″022); fluxes are in arbitrary units.

ergs cm^{-2} s^{-1}. Since the ratio between the two oxygen lines is 1:3 our total flux in the [O III] λ5007 line alone is 1.98×10^{-13} h_{50}^{-2} ergs cm^{-2} s^{-1}. We expect our result to fall between the two values measured by Whittle et al. since the relatively low signal-to-noise and high spatial resolution of the *HST* observations render them insensitive to the faint extended emission, and we expect to miss some of the diffuse flux from the halo.

In our observations the two bright components are of a comparable intensity, and this result differs from the observations of Haniff et al. (1988) who found a strong asymmetry, with the east component being the brighter. As noted by those authors, since the west component is blueshifted (De Robertis 1987) with respect to the overall galaxy velocity, the corresponding [O III] wavelength falls in a region of lower instrumental transmission than the east component, and this produces the apparent difference in intensity. This effect is not important in our data since the transmission difference for the two components is smaller than 3%.

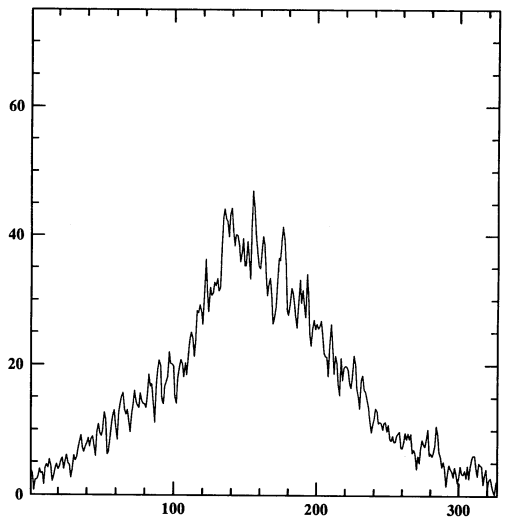

FIG. 3*b*

The biconical structure observed in our [O III] image (Fig. 2) strongly suggests that the origin of the ionization is a central and compact source whose emission is restricted to a well-defined solid angle by a parsec-size thick accretion torus; the cone opening angle is $\alpha = 40° \pm 5°$. This allows us to use the apex of the cone as a reference for position since we expect this point to be coincident with the central ionizing source.

An interesting feature is the obscured region at the cone apex: its angular size is 0.″8 (corresponding to 900 h_{50}^{-1} pc) in the direction perpendicular to the cone axis. From Figure 3, it is evident that the emission seen in F502M between the E and W component is due to continuum radiation: this region shows a "normal" continuum intensity profile with the maximum emission falling in the [O III] obscured region; on the other hand no emission was detected in the UV (1300 Å) observation. These results clearly suggest the geometry of this region; obscuring material prevents the UV emission from the central ionizing source to escape along the line of sight; the same thing happens to any [O III] emission from the innermost gas. The continuum (starlight) emission on the other hand comes from an external region, and it is not affected by the nuclear obscuring material.

The large size of the [O III] obscured region, 900 h_{50}^{-1} pc, suggests that absorbing material (i.e., dust) is required on a much larger scale in addition to the torus (few parsecs size) obscuring the Seyfert 2 nucleus. The geometry of the obscuring material must be related to, or even determined by, the central torus, since otherwise we would require two different obscuration mechanisms, one for the nuclear ionizing source and the other for the central region. For example, the anisotropic emission from the nuclear source can evaporate the dust only along the cone defined by the torus; alternatively the pressure of the nuclear radiation can accelerate the dust away from the nucleus, producing an overall outflow of dust and gas within the cone. Also the radio-emitting plasma can clear a channel along its path: this interpretation is favored by the study of Pogge (1989) who found a strong correlation between the presence of extended radio and [O III] emission. This scenario would require a close alignment between the radio and optical emission which, as we discuss in the following, is not observed for Mrk 78.

The asymmetry of the obscuring region with respect to the cone's apex (and thus to the central source) can be explained even in a symmetrical geometry for the central region: if the angle β between the projection of the cone axis on the sky and the line of sight is not 90°, it will shadow a larger fraction of the lobe away from us than that of the lobe closer to us. Using a simple spherical model (see Fig. 4) and for $\beta < 90° - \alpha$, we obtain that $\beta = \arcsin(r) + \alpha$, where r is the ratio between the sizes of the shadow on the two sides of the center of the cone. From our observation we have $r = 0.35 \pm 0.08$, corresponding to $\beta \approx 60°$. An interesting consequence is that the west component would be closer to us; since we also know that it is blueshifted with respect to the galaxy (De Robertis 1987), this would indicate that we are observing outflowing gas. This result is consistent with the asymmetric profile of the [O III] line observed in Mrk 78 by Heckman, Miley, & Green (1984).

The compact [O III] emission is approximatively aligned with the extended halo; a good alignment is also found with the extended narrow line region (ENLR) discovered by Pedlar et al. (1989) and observed on a scale of up to 16 kpc. The difference between these position angles and the value of 84° obtained by Haniff et al. (1988) can be explained by the presence of the asymmetric bright structures observed on the west side of the halo.

The diffuse halo of [O III] emission can be identified with the A component in the spectral analysis of Whittle et al. (1988): it is a broad component ($\approx 8''$ in length) with a normal galactic rotation curve. The high-ionization state of the extended [O III] emission and its alignment with the cone of compact [O III] emission support the idea of a common origin for ionization, that is, photoionization from the nuclear source.

On the other hand, the compact and extended [O III] emission regions show different dynamical behaviors: the gas within the compact region seems to be outflowing from the nucleus, while the extended halo and the ENLR gas (Unger et al. 1986) undergo to a normal galactic rotation.

We can compare our [O III] images with the VLA radio image of Pedlar et al. (1989) at λ 2 cm with 0".15 resolution. The radio image shows a triple structure, dominated by a bright core and with two extended components on the east and west side. There is no correlation between the radio and the emission line morphologies on this small scale: the cone position angle is 67°, while the radio position angle is 89° (Haniff et al. 1988). The asymmetry observed in the [O III] image, with the east component more compact and closer to the nucleus, is the opposite to that of the radio asymmetry. Furthermore, if we assume that the radio core is coincident with the cone apex, the radio emission would lie along the outer edge of the optical emission-line cone.

Finally, we cannot totally exclude an alternative scenario where we may simply be observing the geometry of the [O III] emitting gas: the central region would not be obscured but rather it would not contain gas at the required ionization state. In this case the asymmetry between the two sides would be intrinsic.

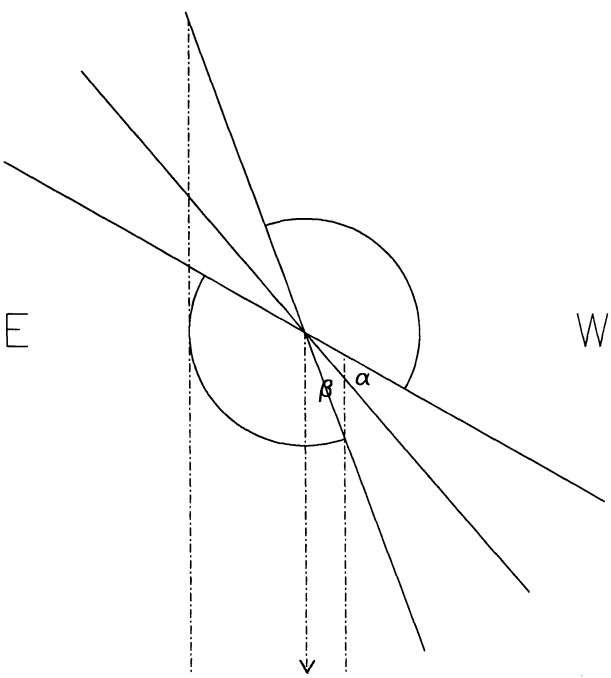

FIG. 4.—Scheme of the obscuration model proposed for Mrk 78

4.2. *The Nuclear Emission*

The misalignment between the emission-line cone and the radio emission suggests that the effects of the relativistic plasma on the ionization of the [O III] emitting gas are not important in Mrk 78.

In the context of pure photoionization, we can estimate the total emission from the nuclear source using the observed NLR luminosity. We assume that the emission from the central source is isotropic, and that can be expressed as a power law, $L_\nu = C\nu^{-\alpha}$, for $\nu_L < \nu < \nu_U$, with $\nu_U \gg \nu_L$ and $\alpha > 1$. The total number of ionizing photons is

$$N_{\rm nuc}(\nu > \nu_0) = \frac{1}{h} C \int_{\nu_0}^{\nu_U} \nu^{-\alpha-1}\, d\nu = \frac{1}{h}\frac{C}{\alpha}\nu_0^{-\alpha}.$$

Only a fraction $\Omega_{\rm NLR}/4\pi$ (the covering factor of the emitting gas) of the emitted photons are absorbed within the NLR. Of course, $\Omega_{\rm NLR} < \Omega$ where Ω is the solid angle subtended by the ionizing cone. An important result of our *HST* observations is a direct estimate for this parameter. From the measured geometrical configuration, we found $\Omega = 0.75$ sr.

The total [O III] emission, not corrected for reddening, is $\log L_{[\rm O\,III]} = 42.61\ h_{50}^{-2}$ ergs s^{-1} (Yee 1980); within the NLR [O III]/H$\beta \approx 10$ (Whittle et al. 1988) and $A_v = 1.05$ (Ferland & Osterbrock 1986), then the estimated Hβ flux is $L = 1.3 \times 10^{42}\ h_{50}^{-2}$ ergs s^{-1}. Using case B recombination, the required number of ionizing photons is $N = 2.1 \times 10^{12} L_{\rm H\beta} = 2.7 \times 10^{54}\ h_{50}^{-2}$ photons s^{-1}.

Finally, the total luminosity of the nuclear source is

$$L_{\rm tot} = C\int_{\nu_L}^{\nu_U} \nu^{-\alpha}\, d\nu = \frac{C}{\alpha-1}\nu_L^{-\alpha+1} = \frac{N}{\Omega_{\rm NLR}}\frac{\alpha}{\alpha-1} h\nu_L \left(\frac{\nu_0}{\nu_L}\right)^{\alpha}.$$

We now compare this result with our UV observations. The nuclear luminosity at $\nu_1 = 1300$ Å (the pivot frequency of the F130M filter) is

$$L_{\nu_1} = \frac{N}{\Omega_{\rm NLR}}\alpha h\left(\frac{\nu_0}{\nu_1}\right)^{\alpha}$$

while we obtained an upper limit of 6.6×10^{25} ergs s^{-1} Hz^{-1}. The ratio R between the observed and computed UV luminosity is

$$R < 6.6 \times 10^{25}\frac{\Omega_{\rm NLR}}{4\pi\alpha h N}\left(\frac{\nu_1}{\nu_0}\right)^{\alpha} \approx 2 \times 10^{-4}\frac{\Omega_{\rm NLR}}{\alpha}.$$

Therefore the observed UV flux is at least three orders of magnitude smaller than required to ionize the NLR. This confirms

the scenario where, due to orientation effects, the active nucleus itself is hidden from view in the case of Seyfert 2 galaxies.

We can also estimate a lower limit to the column density N_H; assuming a standard dust-to-gas ratio ($A_V = 5 \times 10^{-22} N_H$) and applying the reddening curve from Cardelli, Clayton, & Mathis (1989) we find $N_H > 0.5 \times 10^{22}$ cm^{-2}. This lower limit is already much greater than the galactic column density, and it suggests a very high value for N_H, in agreement with those found by Mulchaey, Mushotzky, & Weaver (1992) on a sample of Seyfert 2.

The previous results indicate that most of the emission from the nuclear source is absorbed by an extended dust component, and only a small fraction can escape to ionize the NLR. If the radiation from the nuclear source is absorbed by dust, we expect to observe the far-infrared emission due to the reprocessing of the high-energy photons to lower frequencies.

The amount of radiation absorbed by the dust is given by

$$L_{abs} = \left(1 - \frac{\Omega}{4\pi}\right) L_{tot} = \left(1 - \frac{\Omega}{4\pi}\right) \frac{N}{\Omega_{NLR}} \frac{\alpha}{\alpha - 1} h\nu_L \left(\frac{\nu_0}{\nu_L}\right)^{\alpha} .$$

We can estimate the lower limit to the infrared emission expected in this framework; we adopt $\nu_L = \nu_0$, $\alpha \gg 1$ and $\Omega_{NLR} = \Omega = 0.75$. From a physical point of view, these assumptions correspond to the most efficient nuclear ionizing source, where all of the radiation is emitted at the ionization threshold. Moreover the ionizing flux escaping from the cone must be completely absorbed within the emission-line region. With these values we find $L_{abs} > 9.3 \times 10^{44} h_{50}^{-2}$ ergs s^{-1}. If we drop the initial assumption on the spectrum of the ionizing emission, allowing $\alpha < 1$, we obtain a more general expression for L_{abs} that leads to the same lower limit. Using a slightly different method Storchi-Bergmann, Mulchaey, & Wilson (1992) found an upper limit of $L_{abs} < 2.7 \times 10^{45} h_{50}^{-2}$ ergs s^{-1} that is consistent with our results.

We also estimated L_{abs} assuming a blackbody spectrum. The temperature that minimizes L_{abs} is $T \approx 70{,}000$ K. For $T = 70{,}000$ K, we obtained $L_{abs} = 22 \times 10^{44} h_{50}^{-2}$ ergs s^{-1}.

Our lower limit has to be compared with the observed total far-infrared luminosity $L_{fir} = 4.5 \times 10^{44} h_{50}^{-2}$ (Mazzarella, Bothun, & Boroson 1991): even in the case of a power-law spectrum, L_{abs} is significantly greater than L_{fir}. Moreover, Rowan-Robinson & Crawford (1989) have shown that less than 50% of the far-infrared emission comes from the "Seyfert component", while L_{abs} would be produced within a kpc from the nucleus. Therefore we conclude that the emission seen by the dust must be intrinsically anisotropic.

It has been proposed that bursts of star formation can be an energy source in AGN and that a young stellar population can account for the spectral and energetic characteristics of the nuclear source (Terlevich & Melnick 1986; Terlevich, Diaz, & Terlevich 1990); the anisotropy for an approximately blackbody spectrum, as expected from a stellar population, would have to be even larger to be consistent with the infrared observations, but a burst of star formation is expected to produce isotropic emission. Therefore this mechanism appears not to be important in the case of Mrk 78.

Conversely, the anisotropy can be provided by the configuration of the accretion disk or torus: for example, the inner walls of the torus can act as a mirror, focusing the radiation in a cone with a small opening angle (Sikora 1981; Madau 1988). For example, for a full opening angle of 60°, L_{abs} is decreased by a factor of 13 and would therefore be consistent with the measured far-infrared luminosity.

5. SUMMARY AND CONCLUSIONS

Our *HST* observations show that Mrk 78 has an extended [O III] emission, with a well-defined biconical shape with a full opening angle of 40°. This result is a strong confirmation of the occultation/reflection model for Seyfert 2 galaxies, with a compact central source as the origin for the ionization. The UV emission from this source is obscured, as confirmed by the total lack of far-UV emission in the F130M image.

Dust surrounding the accretion torus is needed to explain the extended obscured central region. The origin for the overall geometric configuration is likely to be connected with the ionizing source and/or with outflowing gas.

The alignment of the extended [O III] emission with the cone of [O III] emission supports the idea of a common origin for the ionization. Nevertheless the compact and extended emitting gas display different dynamic behaviors.

The radio emission is misaligned with respect to the [O III] emission by about 25°; there is no direct morphological association between the radio and [O III] emission. This result strengthens the interpretation of a pure photoionization from a nuclear source as the origin for the overall emission-line region.

In the framework of pure photoionization, we extrapolated the total luminosity of the nuclear source from the luminosity of the emission-line regions. The observed UV flux is at least three orders of magnitude smaller than the flux required to ionize the NLR, corresponding to a column density of $N_H > 0.5 \times 10^{22}$ cm^{-2}.

Moreover, for an isotropic source, the corresponding far-infrared luminosity would greatly exceed the values obtained from the *IRAS* observations; thus we suggest that the dust is heated by a highly anisotropic source, as expected in the case of an accretion torus, with reflecting funnel walls.

REFERENCES

Antonucci, R. R. J., & Miller, J. S. 1985, ApJ, 297, 621
Baldwin, J. A., Wilson, A. S., & Whittle, M. 1987, ApJ, 319, 84
Cardelli, J. A., Clayton, G. C., & Mathis, J. S. 1989, ApJ, 345, 245
Colina, L., Sparks, W. B., & Macchetto, F. 1991, ApJ, 370, 102
De Robertis, M. M. 1987, ApJ, 316, 597
Evans, I. N., Ford, H. C., Kinney, A. L., Antonucci, R. R. J., Armus, L., & Caganoff, S. 1991, ApJ, 369, L27
Ferland, G. J., & Osterbrock, D. E. 1986, ApJ, 300, 658
Haniff, C. A., Wilson, A. S., & Ward, M. J. 1988, ApJ, 334, 104
Heckman, T. M., Miley, G. K., & Green, R. F. 1984, ApJ, 281, 525
Kinney, A. L., Antonucci, R. R. J., Ward, M. J., Wilson, A. S., & Whittle, M. 1991, ApJ, 377, 100
Koski, A. T. 1978, ApJ, 223, 56
Lucy, L. B. 1974, AJ, 79, 745
Madau, P. 1988, ApJ, 327, 116
Mazzarella, J. M., Bothun, G. D., & Boroson, T. A. 1991, AJ, 101, 2034
Miller, J. S., & Goodrich, R. W. 1990, ApJ, 355, 456
Mulchaey, J. S., Mushotzky, R. F., & Weaver, K. A. 1992, ApJ, 390, L69
Paresce, F. 1992, Faint Object Camera Instrument Handbook Version 3.0, Space Telescope Science Institute
Pedlar, A., Meaburn, J., Axon, D. J., Unger, S. W., Whittle, D. M., Meurs, E. J. A., Guerrine, N., & Ward, M. J. 1989, MNRAS, 238, 863
Pogge, R. W. 1989, ApJ, 345, 730
Rowan-Robinson, M., & Crawford, J. 1989, MNRAS, 238, 523
Sikora, M. 1981, MNRAS, 196, 257
Storchi-Bergmann, T., Mulchaey, J. S., & Wilson, A. S. 1992, ApJ, 395, L73
Tadhunter, C., & Tsetanov, Z. 1989, Nature, 341, 422
Terlevich, E., Diaz, A. I., & Terlevich, R. 1990, MNRAS, 242, 271
Terlevich, R., & Melnick, J. 1986, MNRAS, 213, 841
Unger, S. W., Pedlar, A., Booler, R. V., & Harrison, B. A. 1986, MNRAS, 219, 387
Whittle, M., Pedlar, A., Meurs, E. J. A., Unger, S. W., Axon, D. J., & Ward, M. J. 1988, ApJ, 326, 125
Wilson, A. S., Baldwin, J. A., & Ulvestad, J. S. 1985, ApJ, 291, 627
Wilson, A. S., Ward, M. J., & Haniff, C. A. 1988, ApJ, 334, 121
Yee, H. K. C. 1980, ApJ, 241, 894